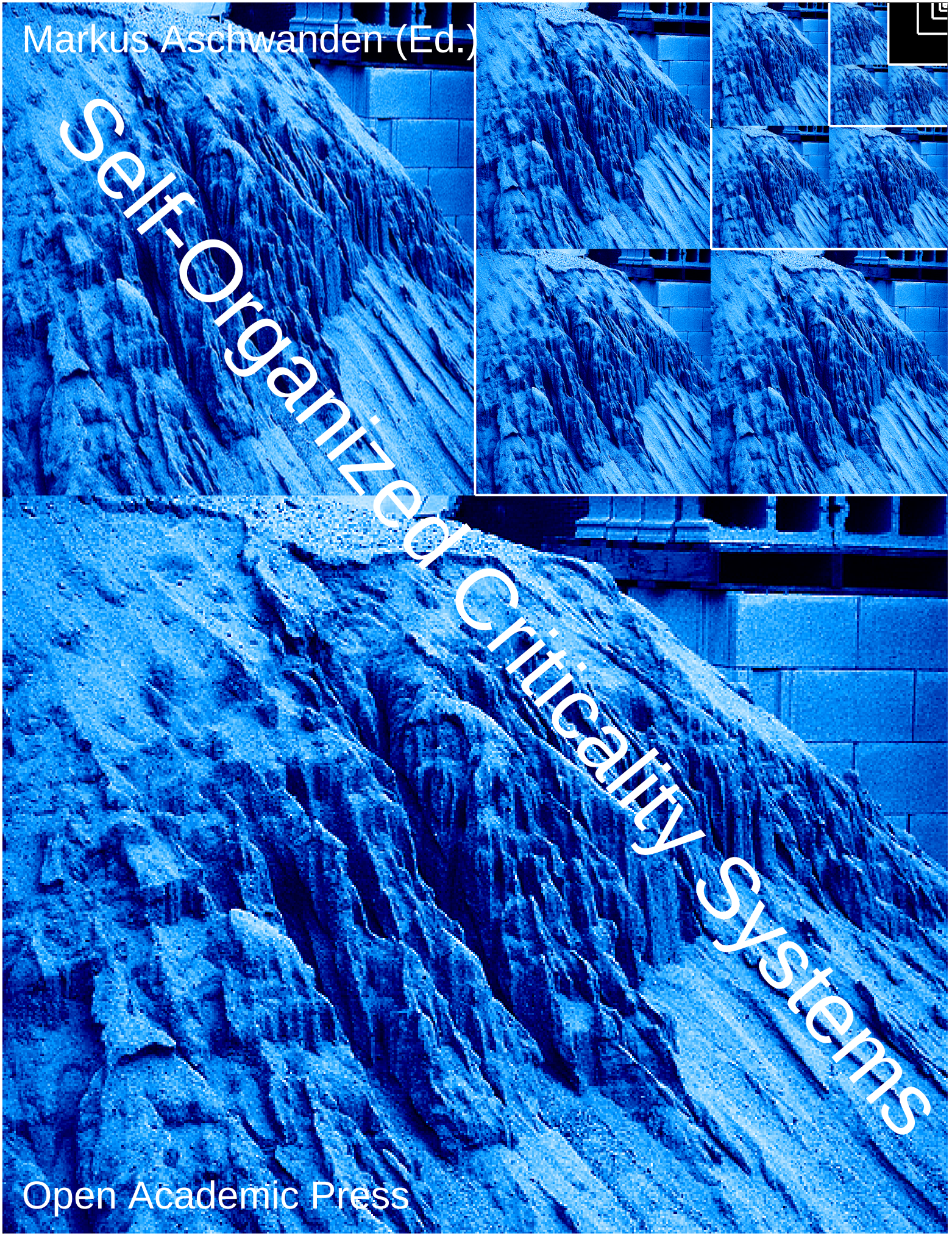
Markus Aschwanden (Ed.)
Self-Organized Criticality Systems
Open Academic Press

Markus J. Aschwanden (Editor)

Open Academic Press Berlin Warsaw 2013

Self-Organized Criticality Systems

Dr. Markus Josef Aschwanden (Editor)
Lockheed Martin, Advanced Technology Center
Solar & Astrophysics Lab, Dept., Org. ADBS, Bldg.252
3251 Hanover Street, Palo Alto, CA 94304, USA
Telephone: 650-424-4001, Fax: 650-424-3994
E-mail: aschwanden@lmsal.com

Published by Open Academic Press Berlin Warsaw 2013
Open Academic Press, Großbeerenstraße 2-10, 12107 Berlin, Germany
Open Academic Press/Villa Europa, ul. Sienna 64, 00-807 Warsaw, Poland
Copyright ©Open Academic Press

All chapters in this book are Open Access distributed under the Creative Commons Attribution 3.0 license, which allows users to download, copy and build upon published articles even for commercial purposes, as long as the author and publisher (Open Academic Press) are properly credited, which ensures max-imum dissemination and a wider impact of our publications. After this work has been published by Open Academic Press, authors have the right to republish it, in whole or part, in any publication of which they are the author, and to make other personal use of the work. Any republication, referencing or personal use of the work must explicitly identify the original source.

Contents

1 Introduction 1
Norma B. Crosby
1.1 A New Theory Emerges 1
1.2 Frequency distribution: a powerful tool 4
1.3 Self-organized criticality and powerlaw behavior 6
1.3.1 Does powerlaw behavior automatically imply SOC? 8
1.3.2 SOC and SOC-like models 9
1.4 Where is SOC observed ? 11
1.4.1 Phenomena on Earth showing SOC behavior 12
1.4.2 Phenomena in space showing SOC behavior 13
1.5 Searching for a common signature: What does it all mean? . 14
References 19

2 Theoretical Models of SOC Systems 23
Markus J. Aschwanden
2.1 Cellular Automaton Models (CA-SOC) 24
2.1.1 Statistical Aspects 25
2.1.2 Physical Aspects 28
2.2 Analytical SOC Models 31
2.2.1 Exponential-Growth SOC Model (EG-SOC) 31
2.2.2 The Fractal-Diffusive SOC Model (FD-SOC) 36
2.2.3 Astrophysical Scaling Laws 45
2.2.4 Earthquake Scaling Laws 47
2.3 Alternative Models Related to SOC 48
2.3.1 Self-Organization Without Criticality (SO) 48
2.3.2 Forced Self-Organized Criticality (FSOC) 49
2.3.3 Brownian Motion and Classical Diffusion 50
2.3.4 Hyper-Diffusion and Lévy Flight 52
2.3.5 Nonextensive Tsallis Entropy 54
2.3.6 Turbulence 55
2.3.7 Percolation 57

2.3.8 Phase Transitions . . . 58
2.3.9 Network Systems . . . 60
2.3.10 Chaotic Systems . . . 61
2.3.11 Synopsis . . . 64
2.4 References . . . 65

3 SOC and Fractal Geometry . . . 73
R. T. James McAteer
3.1 From chaos to order (and back) . . . 74
3.1.1 The coffee table fractal . . . 75
3.1.2 The n-body problem . . . 76
3.1.3 The butterfly effect . . . 77
3.1.4 The critical points . . . 78
3.2 Fractal Properties . . . 79
3.2.1 Dimensionality . . . 80
3.2.2 Self-similarity and Scale-Invariance . . . 81
3.2.3 Generating Fractals . . . 81
3.3 The many flavors of fractal dimension . . . 84
3.3.1 Similarity Dimension of a set of systems . . . 84
3.3.2 Box Counting Dimension . . . 85
3.3.3 The Hölder Exponent . . . 86
3.3.4 The Hurst Exponent . . . 86
3.3.5 Haussdorf Dimension . . . 87
3.4 Multifractals . . . 90
3.4.1 From monofractals to multifractals . . . 90
3.4.2 Generalized Dimensions . . . 91
3.4.3 Connecting forms of multifractality . . . 92
3.4.4 The Devils staircase . . . 94
3.4.5 The Wavelet Transform Modulus Maxima . . . 95
3.5 Future directions . . . 98
References . . . 99

4 Percolation Models of Self-Organized Critical Phenomena 103
Alexander V. Milovanov
4.1 The Percolation Problem . . . 104
4.1.1 Site and Bond Percolation . . . 105
4.1.2 Percolation Critical Exponents β, ν, and μ . . . 106
4.1.3 Random Walks on Percolating Clusters . . . 107
4.1.4 The Spectral Fractal Dimension . . . 108
4.1.5 The Alexander-Orbach Conjecture . . . 108
4.1.6 Percolation Problem on the Riemann Sphere . . . 109
4.1.7 Summary . . . 111
4.2 The SOC Hypothesis . . . 111
4.2.1 SOC vs. Percolation . . . 112
4.2.2 The Guiding Mechanisms . . . 113
4.3 Going With the Random Walks: DPRW Model . . . 114

4.3.1 Description of the Model . . . 115
4.3.2 Random-Walk Hopping Process . . . 116
4.3.3 Dynamical Geometry of Threshold Percolation . . . 117
4.4 Linear-Response Theory . . . 117
4.4.1 Dynamics and Orderings . . . 117
4.4.2 Frequency-Dependent Conductivity and Diffusion Coefficients . . . 118
4.4.3 Power-Law Power Spectral Density . . . 120
4.4.4 Stretched-Exponential Relaxation and the Distribution of Relaxation Times . . . 121
4.4.5 Consistency Check . . . 124
4.4.6 Fractional Relaxation and Diffusion Equations . . . 125
4.4.7 Derivation of the Fractional Diffusion Equation . . . 126
4.4.8 Dispersion-Relation Exponent . . . 127
4.4.9 The Hurst Exponent . . . 128
4.4.10 Activation-Cluster Size Distribution and the τ-Exponent . . . 129
4.4.11 Occurrence Frequency Energy Distribution and the ß-Exponent . . . 129
4.4.12 Values of the Critical Exponents . . . 130
4.5 The Random Walk's Guide to SOC . . . 133
4.5.1 General . . . 133
4.5.2 The Role of Random Walks . . . 134
4.5.3 Universality Class . . . 134
4.6 Self-Organized Turbulence: The "Sakura" Model . . . 135
4.7 Beyond Linear Theories: DANSE Formalism . . . 139
4.7.1 The Roadmap . . . 139
4.7.2 DANSE Equation . . . 141
4.7.3 Coupled Nonlinear Oscillators . . . 142
4.7.4 Chaotic vs. Pseudochaotic Dynamics . . . 143
4.7.5 Nearest-Neighbor Rule . . . 145
4.7.6 Pseudochaotic Dynamics on a Cayley Tree . . . 145
4.7.7 Making Delocalization Transition Self-Organized . . . 148
4.7.8 Asymptotic Spreading of the Hole Wave Function . . . 148
4.7.9 Summary . . . 150
4.8 The Two Faces of Nonlinearity: Instability of SOC . . . 150
4.8.1 Instability Cycle . . . 151
4.8.2 "Fishbone"-Like Instability . . . 154
4.8.3 The Threshold Character of Fishbone Excitation . . . 155
4.8.4 Fractional Nonlinear Schrödinger Equation . . . 156
4.8.5 Mixed SOC-Coherent Behavior . . . 161
4.9 Phase Transitions in SOC Systems . . . 162
4.9.1 Subordination to SOC . . . 163
4.9.2 Generalized Free Energy Expansion . . . 164
4.9.3 Fractional Ginzburg-Landau Equation . . . 164

4.9.4 The q-Exponent . . . 165
4.10 Overall Summary and Final Remarks . . . 166
4.10.1 Finance . . . 169
4.10.2 Climate Dynamics . . . 170
4.11 The Frontier . . . 172
References . . . 174

5 Criticality and Self-Organization in Branching Processes: Application to Natural Hazards . . . 183
Álvaro Corral and Francesc Font-Clos
5.1 The Statistics of Natural Hazards . . . 184
5.1.1 The Gutenberg-Richter Law . . . 184
5.1.2 A First Model for Earthquake Occurrence . . . 187
5.2 Branching Processes . . . 188
5.2.1 Definition of the Galton-Watson Process . . . 189
5.2.2 Generating Functions . . . 189
5.2.3 Distribution of Number of Elements per Generation 192
5.2.4 Expected Number of Elements per Generation . . . 192
5.2.5 The Probability of Extinction . . . 193
5.2.6 The Probability of Extinction for the Binomial Distribution . . . 195
5.2.7 No Stability of the Population . . . 196
5.2.8 Non-Equilibrium Phase Transition . . . 197
5.2.9 Distribution of the Total Size of the Population: Binomial Distribution and Rooted Trees . . . 199
5.2.10 Generating Function of the Total Size of the Population . . . 204
5.2.11 Self-Organized Branching Process . . . 207
5.2.12 Self-Organized Criticality and Sandpile Models . . . 209
5.3 Conclusions . . . 213
Appendix . . . 214
References . . . 226

6 Power Laws of Recurrence Networks . . . 229
Yong Zou, Jobst Heitzig, Jürgen Kurths
6.1 Introduction . . . 229
6.2 Power-law scaling and singularities of the invariant density . 231
6.2.1 One-dimensional maps: Analytical theory . . . 233
6.2.2 Example: Generalized logistic map . . . 235
6.3 Power-laws and fixed points in 2D flows . . . 237
6.4 Power-law scaling versus fractal dimension . . . 238
6.5 Technical aspects . . . 241
6.5.1 Estimation of scaling exponents . . . 242
6.5.2 Selection of dynamical variable . . . 243
6.6 Conclusions . . . 245
References . . . 246

7 SOC computer simulations ... 251
Gunnar Pruessner
7.1 Introduction ... 251
7.1.1 Observables ... 255
7.1.2 Models ... 256
7.2 Scaling and numerics ... 272
7.2.1 Simple scaling ... 273
7.2.2 Moment analysis ... 278
7.2.3 Statistical errors from chunks ... 282
7.3 Algorithms and data organisation ... 284
7.3.1 Stacks ... 285
7.3.2 Sites and Neighbours ... 290
7.3.3 Floating Point Precision ... 294
7.3.4 Random Number Generators ... 295
7.3.5 Output ... 297
7.4 Summary and conclusion ... 300
Appendix: Implementation details for binning ... 301
References ... 303

8 SOC Laboratory Experiments ... 311
Gunnar Pruessner
8.1 Introduction ... 311
8.1.1 Identifying SOC in experimental data ... 312
8.1.2 Tools and features ... 314
8.2 Granular Media ... 317
8.3 Systems with internal disorder ... 320
8.4 Mechanical instabilities: Fracture and rapture ... 323
8.5 Biological systems ... 325
References ... 327

9 Self-Organizing Complex Earthquakes: Scaling in Data, Models, and Forecasting ... 333
Michael K. Sachs, John B. Rundle, James R. Holliday, Joseph Gran, Mark Yoder, Donald L. Turcotte and William Graves
9.1 Introduction ... 334
9.2 Earthquakes ... 335
9.3 Characteristic Earthquakes ... 337
9.4 Models of Earthquakes ... 342
9.5 Forecasting ... 343
9.6 Results ... 352
9.7 Summary ... 354
References ... 354

10 Wildfires and the Forest-Fire Model 357
Stefan Hergarten
10.1 The Forest-Fire Model 358
10.2 Numerical and Theoretical Results 359
10.3 The Relationship to Real Wildfires 364
10.4 Extensions of the Forest-Fire Model 368
References 375

11 SOC in Landslides 379
Stefan Hergarten
11.1 Landslide Statistics 382
11.2 Mechanical Models 386
11.3 Geomorphic Models 390
References 399

12 SOC and Solar Flares 403
Paul Charbonneau
12.1 Introduction: solar magnetic activity and flares 403
12.2 Parker's coronal heating hypothesis 406
12.3 SOC Models of solar flares 410
12.3.1 The Lu & Hamilton model 410
12.3.2 Sample results 413
12.4 Physical interpretation 416
12.4.1 The lattice and nodal variable 417
12.4.2 The stability criterion 417
12.4.3 Computing the released energy 418
12.4.4 Nodal redistribution as nonlinear diffusion 419
12.4.5 Reverse engineering of discrete redistribution rules . 421
12.5 Beyond the sandpile 423
12.5.1 Numerical simulations 424
12.5.2 SOC in reduced MHD 426
12.5.3 Fieldline-based models 427
12.5.4 Loop-based models 429
12.6 Outlook 432
12.7 References 433

13 SOC Systems in Astrophysics 439
Markus J. Aschwanden
13.1 Theory 440
13.1.1 The Scale-Free Probability Conjecture 441
13.1.2 The Fractal-Diffusive Spatio-Temporal Relationship 443
13.1.3 Size Distributions of Astrophysical Observables 445
13.1.4 Scaling Laws for Thermal Emission of Astrophysical Plasmas 448
13.1.5 Scaling Laws for Astrophysical Acceleration Mechanisms 450

13.2 Observations 451
13.2.1 Lunar Craters 452
13.2.2 Asteroid Belt 454
13.2.3 Saturn Ring 455
13.2.4 Magnetospheric Substorms and Auroras 457
13.2.5 Solar Flares 458
13.2.6 Stellar Flares 465
13.2.7 Pulsars 468
13.2.8 Soft Gamma-Ray Repeaters 470
13.2.9 Black Hole Objects 470
13.2.10 Blazars 473
13.2.11 Cosmic Rays 473
13.3 Conclusions 475
13.4 References 478

Chapter 9
Self-Organizing Complex Earthquakes: Scaling in Data, Models, and Forecasting

Michael K. Sachs, John B. Rundle, James R. Holliday, Joseph Gran, Mark Yoder, Donald L. Turcotte and William Graves

Abstract In many natural and social systems, observations of the frequency-size distributions of events can be approximated by power-law (scaling or fractal) distributions. An important question is whether the probability of extreme events can be estimated by extrapolating the power-law distributions, or whether the largest events occur more frequently than the power-law extrapolation would predict. In this paper we consider specifically earthquake systems, and discuss both the data supporting these ideas, as well as simple models. Extrapolations using power-laws are widely used in probabilistic hazard assessment. As a result, the existence of events not falling on the scaling line will be misrepresented by these simple models. We also discuss earth-

Michael K. Sachs
Department of Physics, University of California, Davis, CA e-mail: mksachs@ucdavis.edu

John B. Rundle
Department of Physics, University of California, Davis, CA e-mail: jbrundle@ucdavis.edu

James R. Holliday
Department of Physics, University of California, Davis, CA e-mail: jrholliday@ucdavis.edu

Joseph Gran
Department of Physics, University of California, Davis, CA e-mail: jdgran@ucdavis.edu

Mark Yoder
Department of Physics, University of California, Davis, CA e-mail: mryoder@ucdavis.edu

Donald L. Turcotte
Department of Geology, University of California, Davis, CA e-mail: dlturcotte@ucdavis.edu

William Graves
Open Hazards Group, Davis, CA e-mail: graveswr@gmail.com

Self-Organized Criticality Systems - Dr.Markus J. Aschwanden (Ed.)
Copyright ©Open Academic Press, www.openacademicpress.de

quake forecast models that arise from scaling ideas, specifically the Natural Time Weibull (NTW) model. This idea is based on the premise that the scaling distribution is eventually filled in by smaller events following a previous large event. We illustrate these results by direct application to California and Japan.

9.1 Introduction

Extreme events are large fluctuations that occur suddenly against a background of smaller events. Details of the nature of such events have been discussed recently in Sachs et al. (2012). The statistics of extreme events have been studied extensively (Kinnison 1985). Applications include floods, wars, financial crashes, and many others. Extreme events that change global society were characterized as black swans by Taleb (2007). The frequency-size distributions associated with many natural hazards satisfy power-law (fractal) statistics to a good approximation (Turcotte 1997). They have also been cited as examples of Self-Organized Criticality (SOC). Examples include earthquakes, landslides, volcanic eruptions, and wildfires. In the financial markets, the largest events correspond to financial crashes of markets, currency valuations, and bankruptcy of the largest corporations or financial institutions (Mantegna & Stanley 2000, Sornette 2004). In this paper, we are interested not so much in the scaling behavior itself, but in the departures from pure scaling or SOC.

Forecasting future events generally relies on pattern matching to previous histories of events. An important question in probabilistic hazard assessment is whether future extreme events can be forecast by extrapolating the power-law behavior, and whether the largest outliers recur in some kind of predictable fashion.

In some cases small events satisfy power-law scaling but one or more extreme events are significantly larger than the extrapolation of the power-law scaling. Sornette (2009) refers to this class of extreme events as dragon kings, but they may be more commonly known as nucleation events, or first order phase transitions. Examples might be the population of London and Paris relative to the power-law distribution of the population of the other cities in the U.K. and France. Another example is material fracture. When stress on a brittle material is increased there is often a power-law distribution of acoustic emissions before an unstable fracture propagates through the sample (Guarino et al. 1998). The precursory emissions are a nucleation process and the fracture can be classified as a phase change (Alava et al. 2006).

We will address the question: Are these off-scaling events relevant to probabilistic hazard assessment, or are they inherently unpredictable? Our discussion will emphasize seismic hazard and to a lesser extent, financial hazard.

On relatively large geographic scales the frequency-rupture-area statistics of earthquakes are well represented by power-law statistics even for the largest events. However, this behavior does not seem to be the case locally. On major faults, such as the San Andreas in California, seismic activity is dominated by great earthquakes, like the 1906 San Francisco earthquake. These are known as "characteristic" earthquakes. As a specific example we will consider a characteristic earthquake cycle on the Parkfield segment of the San Andreas fault. We will then consider in some detail the use of slider-block models to represent seismicity.

In the financial area, the tail of the distribution of market moves in the Standard and Poors 500 index is represented by a power-law. The distribution itself is known to be leptokurtotic (Mantegna & Stanley 2000), meaning that the central part of the statistical distribution of price moves is higher than the corresponding Gaussian distribution, but the tails are fatter. Some of the largest moves, such as the famous market crash of October 19, 1987, are outliers on the general trend of power-law scaling (Sornette 2004). They are therefore candidates for nucleation, or dragon king events.

9.2 Earthquakes

The frequency-magnitude statistics of earthquakes have been recognized to satisfy log-linear scaling both globally and regionally. It is widely accepted that earthquakes satisfy the Gutenberg-Richter (GR) scaling relation (Gutenberg & Richter 1954):

$$\log N = a - bm, \tag{9.1}$$

where N is the cumulative number of earthquakes in a region and time interval with magnitudes greater than m. The scaling relation given in equation (9.1) has been shown to be equivalent to a power-law scaling between N and A_r, the earthquake rupture area (Turcotte 1997):

$$N \sim A_r^{-b}. \tag{9.2}$$

Thus earthquakes satisfy power-law scaling. Great earthquakes will be nucleation events or "characteristic earthquakes" if their magnitude significantly exceed the extrapolated scaling relation given in equation (9.1).

In this section we will consider global seismicity. Because of the many problems associated with the magnitudes of large earthquakes, the preferred approach to global seismicity is to use the Global Central Moment Tensor catalog (`www.globalcmt.org`) Dziewoński et al. (1981), Ekström et al. (2005). We utilize this catalog for the period January 1, 1977 to September 30, 2010. In order to update our results through August 15, 2011 we use moment magnitudes given in the ANSS catalog (`www.ncedc.org/cnss/`). Using

these catalogs the cumulative number of global earthquakes with magnitudes greater than for the period 1977 to August 15, 2011 is given in Figure 9.1. The roll over for small magnitudes $m_w \leq 5.25$ is attributed to the sensitivity limit of the global network used to obtain moment magnitudes m_w Engdahl et al. (1998). The roll over for $m_w \geq 7.5$ is more controversial (Rundle 1989, Sornette et al. 1996). It is usually attributed to the transition from small earthquakes with near equal lengths and depths to large earthquakes with lengths much larger than depths.

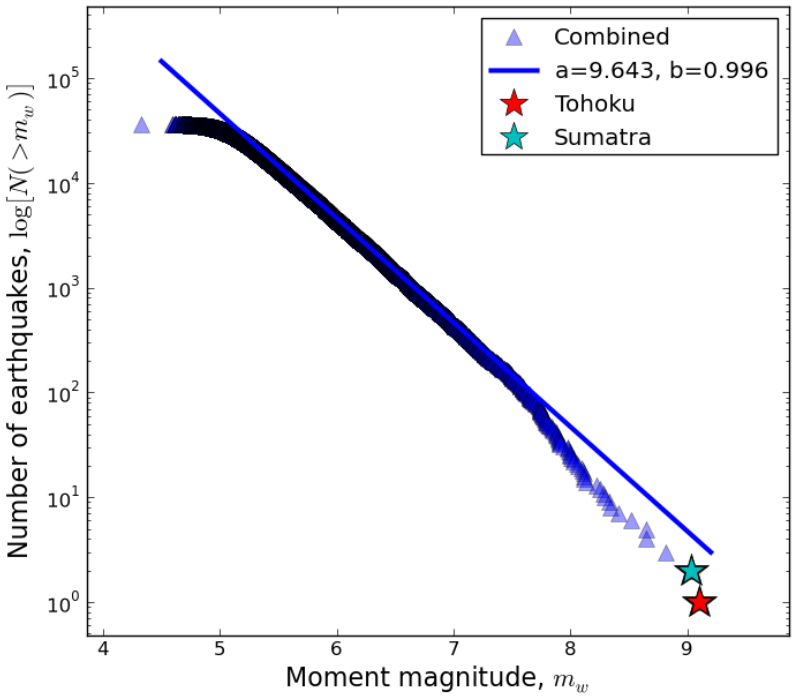

Fig. 9.1: Cumulative number of global earthquakes with magnitude greater than m_w are given as a function of moment magnitudes m_w. Observed values for the period January 1, 1977 to September 30, 2010 are obtained from the global CMT catalog, values for the period October 1, 2010 to August 15, 2011 are obtained from the ANSS catalog. The least-squares best fit of equation (9.1) to the values in the range $5.5 \leq m_w \leq 7.5$ is given taking $a = 9.643$ and $b = 0.996$. Also included are the 2004 $m_w = 9.1$ Sumatra earthquake and the 2011 $m_w = 9.1$ Tohoku earthquake.

Included in Figure 9.1 is the least squares fit of equation (9.1) to the data taking $a = 9.643$ and $b = 0.996$. The fit is carried out between $m = 5.5$ and 7.5 and includes some 30,000 earthquakes. Also included in Figure 9.1 are the $m_w = 9.1$ Sumatra earthquake on December 26, 2004 and the $m_w = 9.1$ Tohoku (Japan) earthquake on March 11, 2011. These were the largest earthquakes during the study period. The tsunami generated by the Sumatra earthquake killed some 230,000 people. The earthquake and tsunami generated by the Tohuko earthquake killed some 22,000 people. In addition the tsunami resulted in a nuclear meltdown at the Fukushima power plant (Hirose 2012). This meltdown created serious economic disruption in Japan and threatens to curtail the global use of nuclear power plants to reduce the emission of greenhouse gasses. The size and impact of the Sumatra and Tohoku earthquakes clearly qualify them as black swans. However, since they lie below the extrapolation of the power-law scaling they would not be considered nucleation events or characteristic earthquakes on a global scale. We will argue in the next section that earthquakes do exhibit characteristic behavior on a regional scale.

9.3 Characteristic Earthquakes

There are two limiting hypotheses for the behavior of faults. In the first, each fault (or fault segment) has a sequence of earthquakes that rupture the entire fault (or fault segment). The global GR (power-law, fractal) distribution of earthquakes illustrated in Figure 9.1 is attributed to a power-law (fractal) distribution of fault areas. Each fault has an earthquake with rupture area equal to the area of the fault. In seismology these are known as "characteristic" earthquakes. The other limiting hypothesis is that every fault has a GR distribution of earthquake magnitudes. The global GR scaling is the sum of the GR scaling on individual faults. The actual behavior of the earth lies between these two limits (Wesnousky 1994).

Ideally, observations would discriminate between the two limiting hypotheses. However, it is impossible to attribute smaller earthquakes to specific faults because only the largest faults can be mapped and identified. Also, location errors of smaller earthquakes make their association with each other and individual faults very difficult. The generally accepted view in seismology is that smaller earthquakes on a fault obey power-law (GR) scaling but a large fraction of the deformation on the fault is associated with large quasi-periodic "characteristic" earthquakes. Thus these large characteristic earthquakes satisfy the condition to be fault-wide nucleation events. Wesnousky (1994) has given data to support the generally accepted view that a working definition of characteristic earthquakes is that they are large earthquakes on plate-boundary faults. As examples we consider two major plate-boundary faults: *1*) The San Andreas fault in California is a major boundary fault be-

tween the Pacific and North American plates and *2*) the subduction zone fault (unnamed) above the Pacific plate as it is being subducted beneath Japan.

A comprehensive study of characteristic earthquakes has been carried out on the southern section of the San Andreas fault. Paleoseismic studies using radiocarbon dating of fluidized sediments at the Wrightwood site (Biasi et al. 2002) date characteristic earthquakes at (in years CE): 534 (407-628), 634 (551-681), 697 (657-722), 722 (695-740), 781 (736-811), 850 (800-881), 1016 (957-1056), 1116 (1047-1181), 1263 (1191-1305), 1487 (1448-1518), 1536 (1508-1569), 1685 (1647-1717), 1812 (historic), 1857 (historic). The ranges of values are the 95% confidence intervals on the radiocarbon dates. The 1857 earthquake was an historic earthquake that ruptured some 400km of the fault from central California to the Los Angeles area. No seismic recordings were available at the time of this earthquake but measurements of surface displacements indicate a magnitude $m \simeq 8.2$. In the past 75 years no earthquake with $m > 5.5$ has occurred on this fault segment. If GR scaling were valid for this fault, there should be approximately 500 $m > 5.5$ earthquakes for each $m = 8.2$ earthquake. These cannot all be in the form of aftershocks, because Bath's law (Scholz & Anderson 2002) implies that the largest aftershock should be approximately $m \simeq 7$. For this largest aftershock, GR scaling then implies that there should be approximately 10 $m > 6$ aftershocks, approximately 100 $m > 5$ aftershocks, and so on. Even accounting for aftershocks of aftershocks, it is unlikely that the aftershock sequence will have 500 $m > 5.5$ events.

Seismologists generally accept that the sequence of paleo-earthquakes listed above are characteristic earthquakes (Scholz & Anderson 2002, Wesnousky 1994). Similarly the 1906 earthquake that destroyed San Francisco is generally accepted to be a characteristic earthquake on the northern San Andreas fault. However, paleoseismic sites are not available on the rupture zone of this earthquake.

Similar paleoseismic studies have dated characteristic earthquakes on the southern Nankai Trough segment of the subduction zone beneath Japan. Characteristic earthquakes occurred in 684, 887, 1099, 1361, 1605, 1707, 1854, and 1946. The dates for these earthquakes were obtained using a variety of historic and other records (Ando 1975). The Tohoku earthquake was a characteristic earthquake on the northern section of this fault and is similar to the San Francisco earthquake in that paleoseismic data are not available (Wesnousky 1994).

The best documented sequence of characteristic earthquakes occurred on the Parkfield segment of the San Andreas fault in California. Evidence suggests that earthquakes with $m \simeq 6$ occurred in 1857, 1881, 1901, 1922, 1934, 1966, and 2004 (Bakun et al. 2005). Based on seismograms the 1922, 1934, 1966, and 2004 events were remarkably similar in magnitude. The Parkfield earthquakes are globally unique in that they are a sequence of relatively small plate-boundary "characteristic" earthquakes. Thus they occur frequently and

a complete "characteristic" earthquake cycle can be studied. In order to study the seismicity associated with the 2004 "characteristic" earthquake we consider earthquakes during the period 1972 (five years after the $m = 6.0$, June, 1966 earthquake) to 2009 (five years after the $m = 5.95$, 28 September, 2004 earthquake). To isolate seismicity associated with the characteristic Parkfield earthquake we confine our study to the region where aftershocks of the 2004 earthquake were concentrated (Shcherbakov et al. 2006).

The region is elliptical, centered at 35.9°N and -120.5°W with semi-major and semi-minor axes of 0.4° and 0.15° respectively, oriented at 137°NW. Both the aftershocks and the elliptical region are shown in Figure 9.2. It is standard practice to associate the aftershock regions with correlated seismicity to study a characteristic earthquake (Hofmann 1996, Ishibe & Shimazaki 2009, Wesnousky 1994). Another advantage of the Parkfield region is the localization of the correlated seismicity. This region clearly excludes the aftershocks of the $m = 6.5$ (2004) San Simean earthquake (lower left hand corner in Figure 9.2 and the aftershocks of the $m = 6.5$ (1983) Coalinga earthquake (just above the red elliptical area).

Parkfield is the site of the highest quality local seismic network in the world (Bakun et al. 2005). This network was constructed by the U.S. Geological Survey in the 1980's in the expectation that the next characteristic earthquake would occur. In our analysis we have used the catalog provided by the Northern California Earthquake Data Center (NCSN catalog, `http://quake.geo.berkeley.edu/ncedc/`) .

The cumulative frequency-magnitude distribution of earthquakes in the Parkfield aftershock region for the period 1972 to 2009 is given in Figure 9.3. The best-fit scaling to this distribution is given by equation (9.1) with $a = 5.65$ and $b = 1$. This is the least-squares best fit to the data in the range $2.5 \leq m \leq 4.5$. Over this range there are some 3,000 data points. The roll over for $m \leq 2.5$ is attributed to a lack of sensitivity of the network for small magnitudes (Shcherbakov et al. 2006). The roll over for $m \geq 4.5$ is attributed to the relatively small number of earthquakes: $N \sim 10$ (Shcherbakov et al. 2006).

If this scaling was applicable to the characteristic earthquake ($N = 1$) it's magnitude would have been $m = 5.65$. The $m = 5.95$ Parkfield main shock clearly lies above the extrapolation of the power-law correlation of the smaller earthquakes. An important question is whether the difference between $m = 5.65$ and $m = 5.95$ can be attributed to the statistical variability of the characteristic earthquakes. Excellent seismic records are available for the 1934, 1966, and 2004 characteristic earthquakes. The magnitudes are $m = 6.0 \pm 0.1$. In addition the seismic records of the 1934 and 1966 earthquakes are essentially identical indicating near identical points of rupture initiation and propagation pattern. The 2004 earthquake has a somewhat different rupture pattern but the rupture zone is considered to very nearly identical to the earlier earthquakes. The evidence is that these are truly characteristic earthquakes that rupture the same specified segment of the San

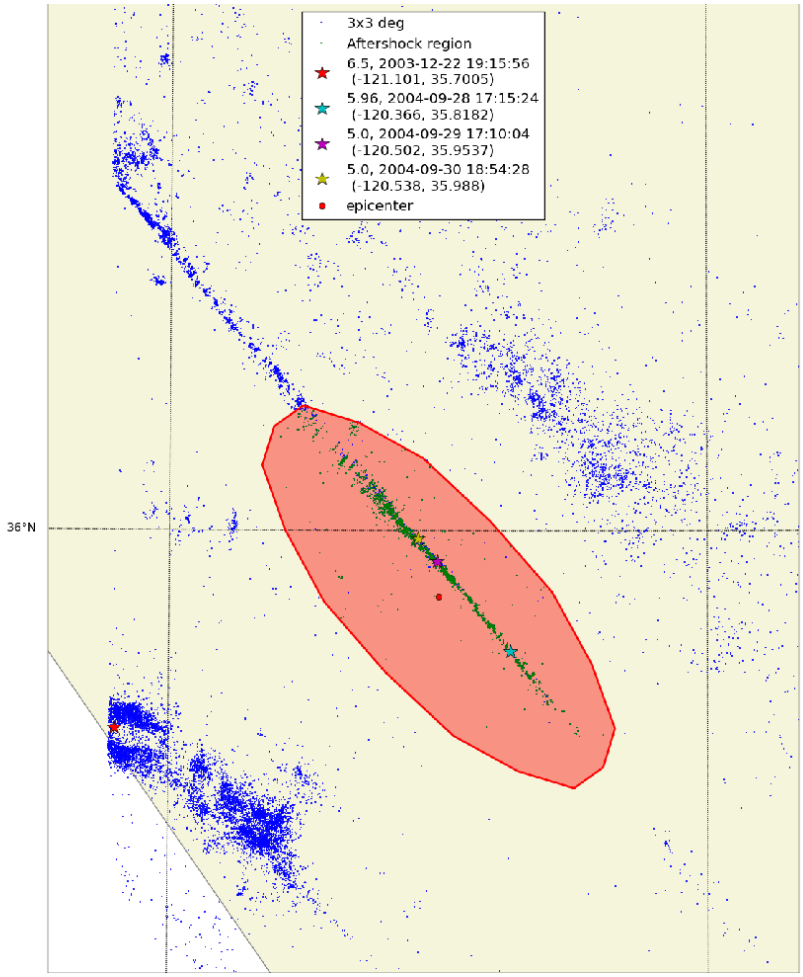

Fig. 9.2: Seismicity in central California for the period 28 September, 1999 to 28 September 2009. The aftershocks of the 18 September, 2004 Parkfield earthquake are shown in the red elliptical area. Aftershocks of the 2004 San Simean earthquake and residual aftershocks of the 1983 Coalinga earthquake are clearly seen to the south-west and north-east of the study region.

Andreas fault. The possibility that one of these characteristic earthquakes could have had a magnitude as low as 5.65 is excluded by the available data. Thus we conclude that the sequence of characteristic earthquakes of the Parkfield segment are dragon kings. Although the $\Delta m = 0.3$ difference between the 2004 Parkfield event and what one would expect from extrapolating the scaling relation in equation may not seem large, it represents about a factor

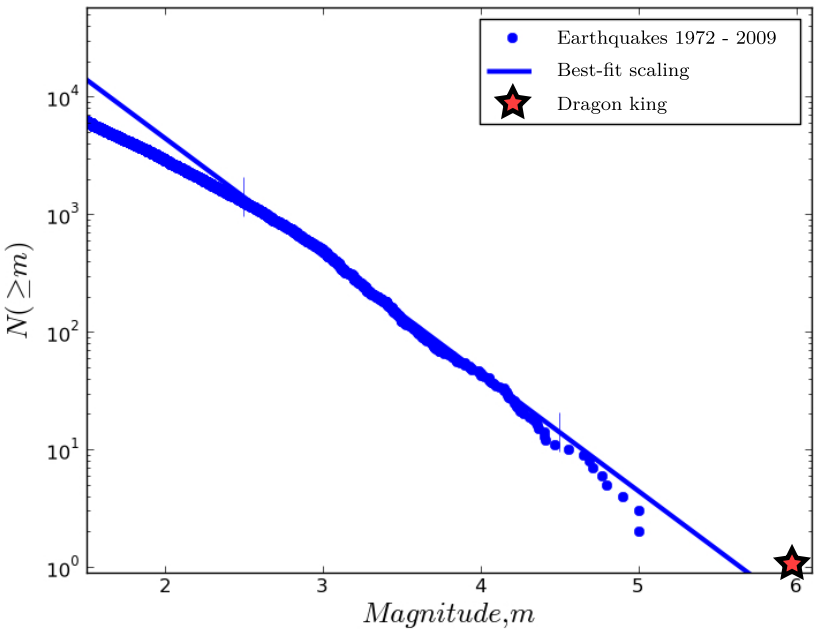

Fig. 9.3: Cumulative number of earthquakes with magnitude greater than m as a function of m for the Parkfield earthquake cycle 1972 to 2009. The best-fit scaling from equation (9.1) is also shown. The $m = 5.65$ Parkfield earthquake is shown as an outlier, sometimes called a "Dragon King".

of three difference in energies which does set it above the extrapolated GR background.

For reasons stated above the Parkfield characteristic earthquake cycle is the only such cycle that can be studied in detail using a high quality earthquake catalog. However, based on the absence of earthquakes adjacent to other segments of the San Andreas fault and other faults where characteristic earthquakes occur, we conclude that characteristic earthquakes are dragon kings with respect to the correlated seismicity (including aftershocks). The background seismicity satisfies power-law Gutenberg-Richter statistics but the characteristic earthquakes lie above the extrapolation as shown in Figure 9.3.

9.4 Models of Earthquakes

The multiple slider-block model has been proposed as a deterministic example of self-organized critical behavior (Carlson & Langer 1989). This model had previously been proposed as a simple model of earthquake behavior (Burridge & Knopoff 1967). Utilizing the multiple slider-block simulations of Abaimov et al. (2008) we will demonstrate characteristic earthquake behavior. A linear chain of 100 slider blocks was pulled over a surface at a constant velocity by a loader plate as illustrated in Figure 9.4. Each block is connected to the loader plate by a spring with spring constant k_L and adjacent blocks are connected to each other by springs with spring constant k_C. An important parameter in the problem is the ratio of spring constants $\alpha = k_C/k_L$. This is a measure of the stiffness of the system. The blocks interact with the surface through a static-dynamic friction law. With the static coefficient of friction larger than the dynamic (sliding) coefficient of friction, stick-slip behavior is observed. The size of a slip event is given by the number of blocks L that slip simultaneously in the event. The stiffness α acts as a tuning parameter in this problem.

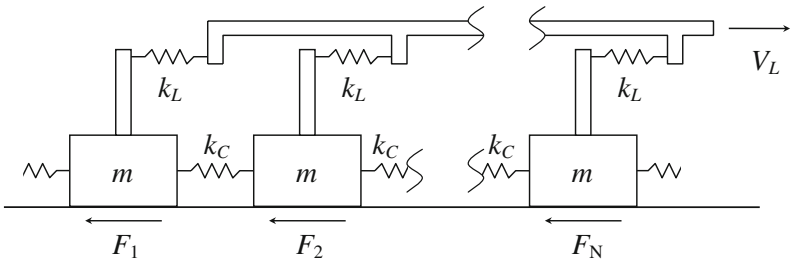

Fig. 9.4: Illustration of the one-dimensional slider-block model. A linear array of N blocks of mass m are pulled along a surface by a constant velocity V_L loader plate. The loader plate is connected to each block with a loader spring with spring constant k_L and adjacent blocks are connected by springs with spring constant k_C. The frictional resisting forces are F_1, F_2, ..., F_N.

For soft systems (α small) only small slip events occur, there is an exponential decay for larger slip events. As α is increased system wide ($L = 100$) events begin to occur. The frequency-size distribution of the slip events for a stiff system ($\alpha = 1000$) is given in Figure 9.5. Statistics for 10,000 events are given and about 1,500 are system wide ($L = 100$) events. The small events are well approximated by the power-law relation equation (9.1).

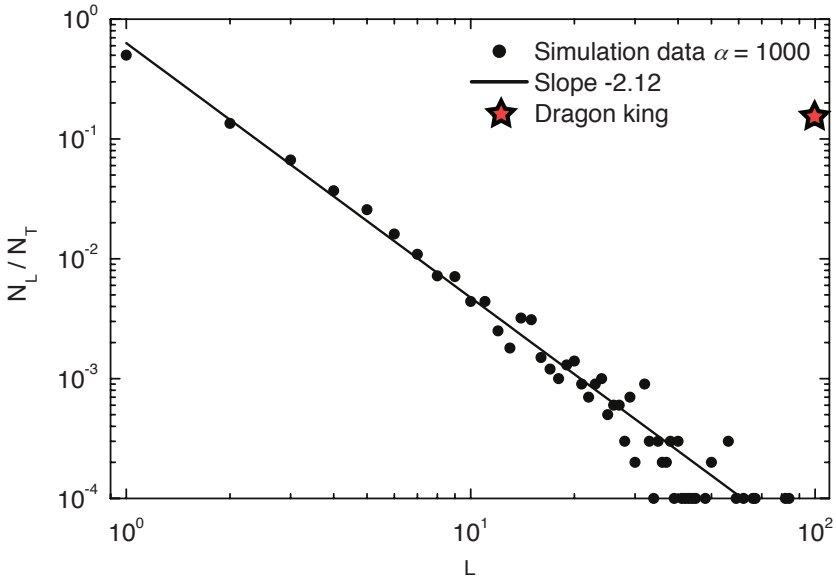

Fig. 9.5: Frequency-size density function of 10,000 slip events for a "stiff" system with $\alpha = k_C/k_L = 1000$. The ratio of the number of events N_L of event size L to the total number of events N_T is given as a function of L. The solid line is a power-law dependence with exponent $-(b+1) = -2.12$. System-wide ($L = 100$) characteristic or "Dragon-King" events are clearly evident.

9.5 Forecasting

Earthquake forecasting is of considerable importance for public safety, and to set earthquake insurance rates (Field 2007a). Recently a series of earthquake forecasts were solicited for a truly prospective forecast evaluation exercise in California (Field 2007b, Lee et al. 2011). This Relative Earthquake Likelihood Model (RELM) exercise led to the submission of nine complete forecasts by six participants for the testing region (primarily California). Participants submitted expected probabilities of occurrence of $m \geq 4.95$ earthquakes in $0.1^\circ \times 0.1^\circ$ cells for the period 1 January 1, 2006, to December 31, 2010. Probabilities were submitted for 7,682 cells in California and adjacent regions. During this period, 31 $m \geq 4.95$ earthquakes occurred in the test region. These earthquakes occurred in 22 test cells. The seismic activity was dominated by earthquakes associated with the $m = 7.2$, April 4, 2010, El Mayor-Cucapah earthquake in northern Mexico. This earthquake occurred

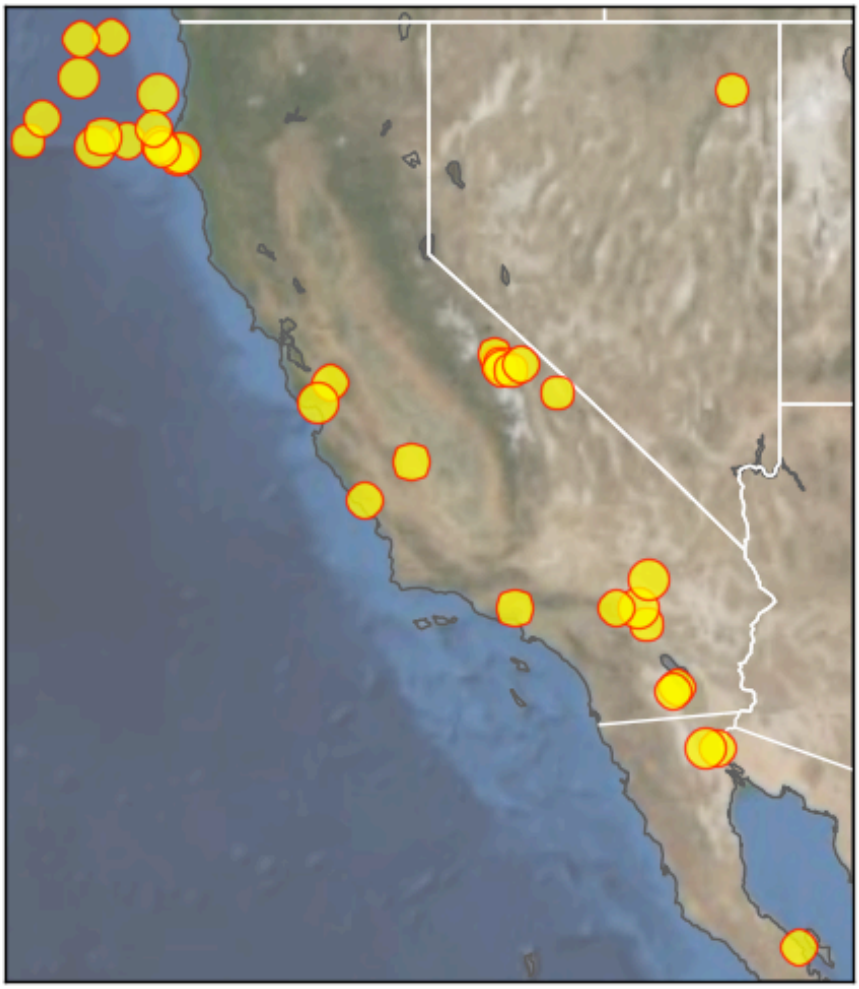

Fig. 9.6: Map of the California-Nevada region showing the epicenters of all $m_l \geq 6$ earthquakes that have occurred in the region from January 1, 1980 through July 17, 2012. Data were obtained from the ANSS catalog.

in the test region, and 16 of the other 30 earthquakes in the test region could be associated with it.

All of these forecasts relied on the Gutenberg-Richter scaling relation to partition the earthquakes into magnitude levels or "bins", and to adjust the projected rates of occurrence of the $m \geq 4.95$ events. The basic idea for most of the forecasts was to project the rate of small earthquakes, which occur at a reasonably steady rate through time, to compute the rate of the large ($m \geq 4.95$) earthquakes.

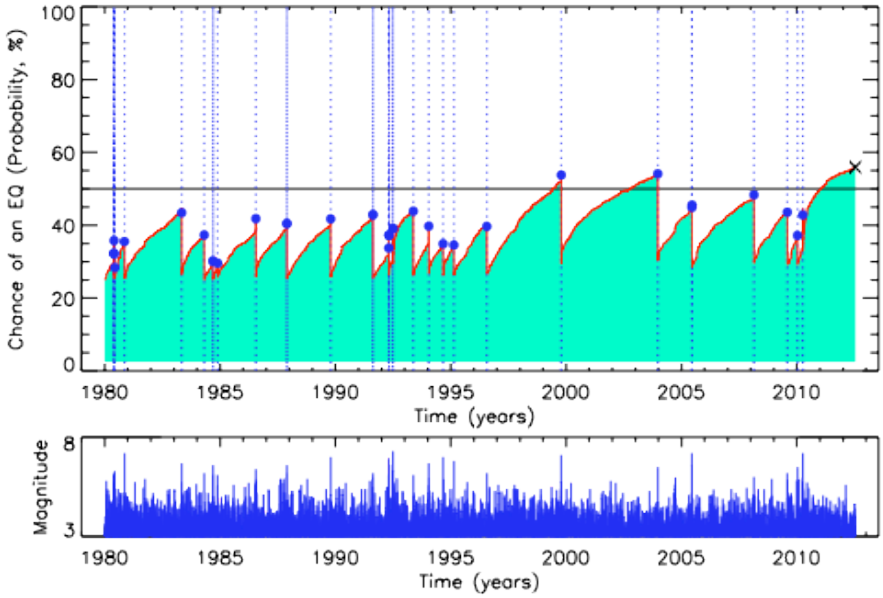

Fig. 9.7: Optimized timeseries for earthquake probabilities in the California-Nevada region. **Top**: Chance of an earthquake having magnitude $m_l \geq 6$ during the next 12 months as a function of time. **Bottom**: Magnitudes of all events in the region as a function of time. Blue dots and vertical dashed lines are earthquakes in the region having $m_l \geq 6$. "X" represents current 12-month probability of ∼56%.

Lee et al. (2011) evaluated the success of the forecasts by means of a test rewarding forecasts for the most accurate locations of the prospective earthquakes. Most of the forecasts were successful in that the great majority of the 31 earthquakes occurred in the highest probability areas. There were several "rogue" earthquakes that occurred in low probability areas, but these were very much the exception.

While this exercise in forecasting the locations of future earthquakes shows considerable promise, less progress has been made on forecasting the time of the next large earthquake in a region. Typically, the assumption is made that earthquakes occur randomly in time and should therefore be described by Poisson statistics. This leads to a probability (Yates & Goodman 2005) for the recurrence of an event during the next time interval Δt:

$$P(t) = 1 - e^{-\nu \Delta t}, \tag{9.3}$$

where ν is the long term Poisson rate of the earthquakes, and Δt is a fixed future time interval. One of the primary justifications for this assumption

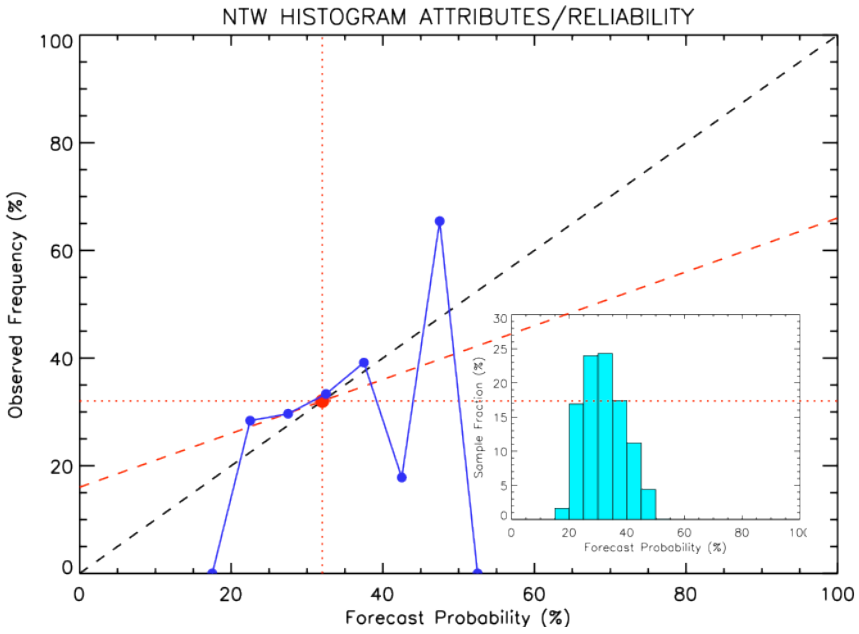

Fig. 9.8: Reliability (scatterplot) diagram for earthquake probabilities corresponding to the timeseries shown in Figure 9.7. In the figure, there are 7 bins having forecast probability, and these are plotted against observed frequencies. A perfectly reliable forecast would have zero reliability error, and the blue dots would lie along the black dashed line having slope = 1. The red dashed line is the no skill line, and the large red dot is the "climatology point", or average forecast. **Inset**: The fraction of samples in each of the 20 forecast bins of 0% to 5%, 5% to 10%, ..., 95% to 100%.

originates in a study by Gardner & Knopoff (1974), in which they removed increasing numbers of "foreshocks" and "aftershocks" from the earthquake catalog until the remaining "main shocks" could be described by a Poisson statistics. Other more recent studies assert that earthquakes should be described by negative binomial statistics (Schorlemmer et al. 2010). It should be recalled that Poisson statistics are meant to describe random events that are IID and uncorrelated such as nuclear decay, assumptions that may be questionable for earthquakes. The existence of aftershocks (e.g., Scholz (1990)) implies that earthquake correlations exist, while observations of progressively propagating mainshocks along the Anatolian fault suggest that major earthquakes are not independent (Stein et al. 1997).

As a result, we are motivated to turn to a new type of forecast, the Natural Time Weibull (NTW) model (Rundle et al. 2012). This model is based on the idea that over any period of time, the distribution of earthquake sizes should most likely be the observed Gutenberg-Richter distribution (equation (9.1)).

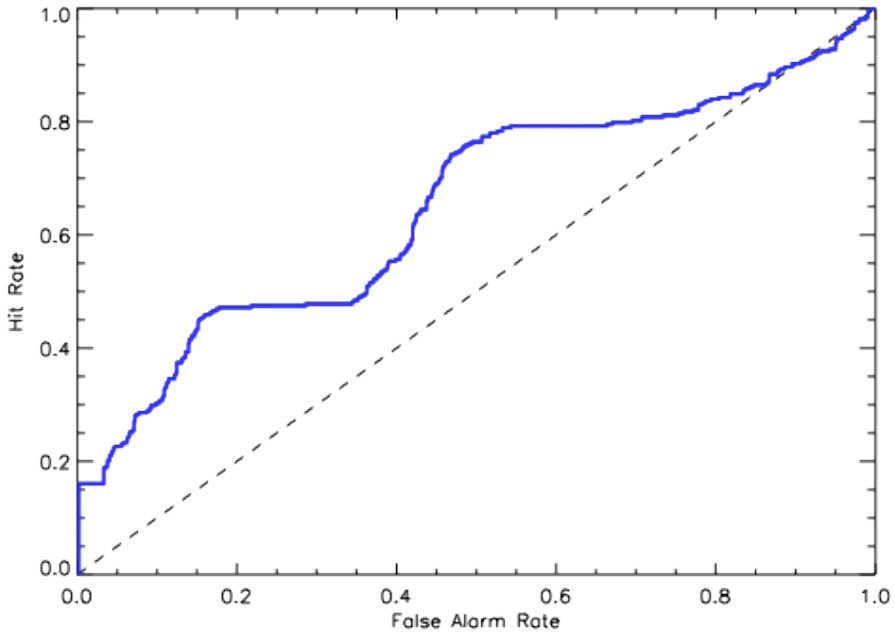

Fig. 9.9: Temporal Receiver Operating Characteristic diagram for the forecast of Figure 9.7. The solid blue line is the ROC diagram for January 1, 1980 through July 17, 2012.

For example, suppose that the large earthquake of interest has magnitude $m_l \geq 6$, and our catalog completeness level is $m_s \geq 3$. Further, suppose that the b-value in the GR relation is the typical value $b = 1$. Then for each $m_l \geq 6$ earthquake we expect 1000 $m_s \geq 3$ earthquakes. Using equation (9.1), we can compute the number of small earthquakes for every large earthquake $N_{ls} = 10^{b(m_l - m_s)}$. Another way of making the same statement is that the natural time scale for the occurrence of large earthquakes is not, in fact, the number of round trips of the earth around the sun (calendar time), but is instead the number of small earthquakes that occur between the occurrence of the large earthquakes. This can be construed as a natural time scale, or alternatively a stress-release time scale. It depends only on the observed fat-tailed statistics of the process, rather than an approximation by the Poisson law.

The NTW method is then based on the idea of counting the number of small earthquakes since the last large earthquake. Once 1000 $m_s \geq 3$ earthquakes have occurred, it is likely that another $m_l \geq 6$ earthquake is due to occur soon. To transform this idea into a probability, we use the Weibull probability law, which is often used in engineering calculations of hazard and

reliability. In the time domain, the Weibull failure law is usually stated as (Evans et al. 2000):

$$P(t) = 1 - e^{-\left(\frac{t}{\theta}\right)^{\beta}}. \tag{9.4}$$

Here t is the time to failure of the test element, θ is a time scale, and β is a constant.

Recalling the previous discussion, we apply the Weibull law (9.4) in the natural time, or event count domain. In addition, we note that earthquakes are a repetitive sequence of events. So we wish to compute the probability of observing the next large event, say $m_l \geq 6$ conditioned on the observation that n smaller events having $3 \leq m_s \leq 6$ since the last large event. In the natural time domain, this requirement leads to the equation:

$$P(\Delta n|n) = 1 - e^{-\gamma\left(\left(\frac{n+\Delta n}{N_{ls}}\right)^{\beta} - \left(\frac{n}{N_{ls}}\right)^{\beta}\right)}. \tag{9.5}$$

Here $P(\Delta n|n)$ is the conditional probability that a large earthquake $m_l \geq 6$ will occur after a number Δn of subsequent small earthquakes $3 \leq m_s \leq 6$ have occurred, given that n small earthquakes have previously occurred since the last large earthquake.

Equation (9.5) does not depend explicitly on time, or on future (calendar) time Δt. To map this probability back to the dual (calendar) time domain, we make the reasonable assumption that for a small time interval Δt:

$$\Delta n \simeq \nu_s \Delta t, \tag{9.6}$$

where ν_s is the Poisson rate of small events computed from having magnitude $3 \leq m_s \leq 6$. Using (9.6) in (9.5), we can estimate the conditional probability in the dual, time domain:

$$P(\Delta t|t) = 1 - e^{-\gamma\left(\left(\frac{n(t)+\nu_s \Delta t}{N}\right)^{\beta} - \left(\frac{n(t)}{N}\right)^{\beta}\right)}. \tag{9.7}$$

Here γ, β are constants.

We now address the question of how to determine the optimal values of γ, β. We first rewrite equation (9.7) as:

$$P(\Delta t|t) = 1 - e^{-H_R(t,\Delta t)}, \tag{9.8}$$

where $H_R(t)$ is the hazard rate (Evans et al. 2000). $H_R(t, \Delta t)$ is a function of time t since the number of small earthquakes since the last large earthquake is a function of time, $n = n(t)$.

We next use the principle that the NTW probability represents a fluctuation around the long-term Poisson rate. Thus we require that:

$$\langle H_R(t, \Delta t)\rangle_T = \nu_s \Delta t. \tag{9.9}$$

Here $\langle ... \rangle_T$ is the time average over a long (multi-decadal) time scale T considered to be much longer than the $m_l \geq 6$ recurrence interval τ:

$$\langle x(t) \rangle_T = \int_{t=-T}^{t=0} x(t')dt', \tag{9.10}$$

$t = 0$ is assumed to be the present.

Using (9.9) and (9.10) together with (9.7) and (9.8), we find that:

$$\gamma = \frac{\nu_s \Delta t}{\left\langle \left(\frac{n(t)+\nu_s \Delta t}{N} \right)^\beta - \left(\frac{n(t)}{N} \right)^\beta \right\rangle_T}. \tag{9.11}$$

Since ν_s and N are assumed to be known, Δt is a chosen time interval, and $n = n(t)$ is known from past data, γ can be determined once β is known.

To determine β, we optimize the probability using standard methods for data assimilation via backtesting with prior data. A considerable literature has accumulated in the weather and financial communities relating to forecast validation (Jolliffe & Stephenson 2011). Of particular interest are Reliability/Attributes (R/A) tests (Hsu & Murphy 1986, Murphy & Daan 1985), and Receiver Operating Characteristic (ROC) tests (Green & Swets 1966, Kharin & Zwiers 2003, Mason 1982, Murphy & Winkler 1987). The R/A test is essentially a scatter plot, in which the frequency of observed large events is plotted against the computed large event probabilities. The ROC test plots successful forecasts (H = "hit rate") against false alarms (F ="false alarm rate"). In the R/A test, reliability is computed by a weighted measure known as the Briar Skill Score (BSS), and is displayed as a scatter plot of observed frequency versus forecast probability (Hsu & Murphy 1986). In the R/A test, the BSS can be decomposed into a set of terms that represent respectively the Reliability, Sample Skill and the Resolution, which are all measures of forecast quality.

While these tests are most often used to evaluate forecasts following the forecast events, they can also be used to assimilate data into the forecast model, thereby optimizing the forecast during backtesting. It is this application that is employed to determine the value γ, β. Details are described in Rundle et al. (2012), but the basic idea is the following.

Using a grid search method, we pick a value of β, then solve (9.11) for γ. We then compute the R/A scatter plot and the ROC plot. Balancing the attributes of reliability, resolution and skill, we repeat the process many times to find an optimal value of β, and from that value, we compute γ via equation (9.11). Our basic result is that, for a broad range of regions, we find a typical optimal value of $\beta = 1.4$. Figures 9.7 - 9.9, 9.11 - 9.13 are computed using this value of β.

There are several ways to estimate uncertainty in the computation of reliability, skill and resolution. The method we use is the bootstrap method, in which large earthquake times are sampled with replacement (Rundle et al.

2011). Estimates of reliability or other parameters are computed for suites of models having the optimal parameters, and the envelope of uncertainty is computed. Details are described in Rundle et al. (2011).

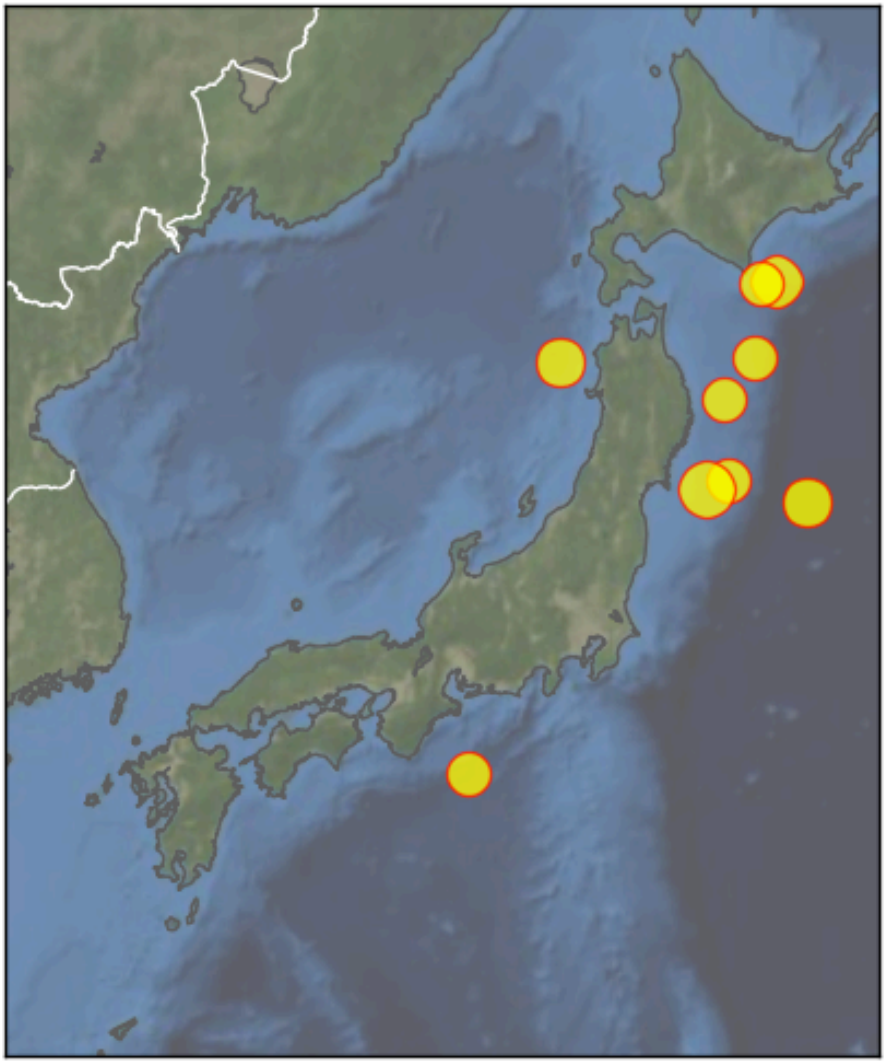

Fig. 9.10: Map of the Japan region showing the epicenters of all $m \geq 7.25$ earthquakes shallower than 40 km depth that have occurred in the region from January 1, 1980 through July 17, 2012. Data were obtained from the ANSS catalog.

In a similar way, we compute a forecast in the Japan region over the period January 1, 1980 - July 17, 2012. This forecast is for $m_l \geq 7.5$ over 4 years (48 months), in the region between latitudes 28° and 42° north, and between longitudes 127° and 146° degrees east. For the Japan calculations, we use $m_s \geq 4.25$, a maximum depth of 40 km (shallow events), and again use a time step of 0.01 year. The map of large events is shown in Figure 9.10, the forecast is shown in Figure 9.11, and the R/A and ROC curves are shown in Figures 9.12 and 9.13. In the Japan figures, the R/A and ROC curve use data only through 06:25:50.30 GMT on March 11, 2011, the date of the great $m = 9.1$ Tohoku, Japan earthquake. Again, the portion of the forecast in Figure 9.11 would be counted as a false alarm by the R/A and ROC methods if we were to use that data in calculations, so again the forecast since March 11, 2011 represents an actual forecast of future activity.

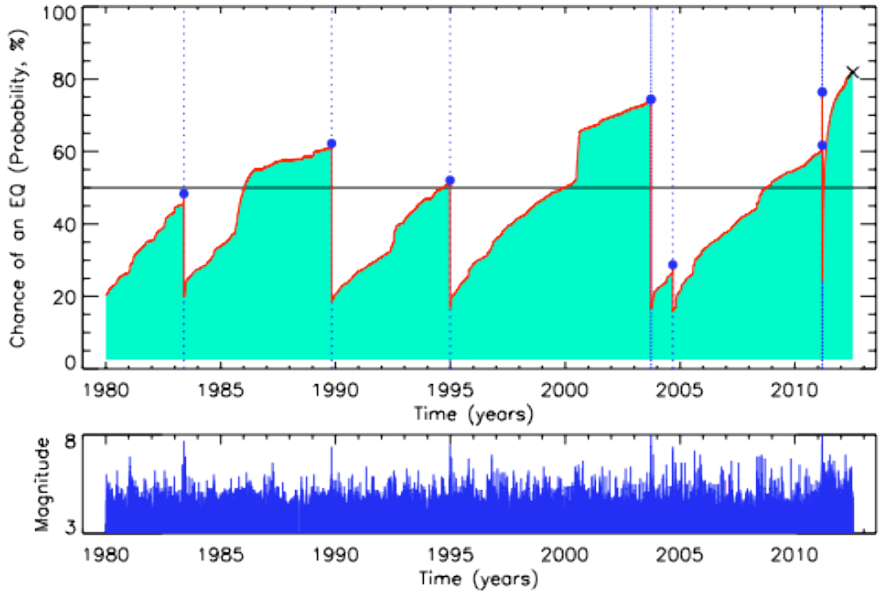

Fig. 9.11: Optimized timeseries for earthquake probabilities in Japan. **Top**: Chance of an earthquake having magnitude $m \geq 7.25$ during the next 48 months as a function of time. **Bottom**: Magnitudes of all events in the region as a function of time. Blue dots and vertical dashed lines are earthquakes in the region having $m \geq 7.25$. "X" represents current 48-month probability of ~83%.

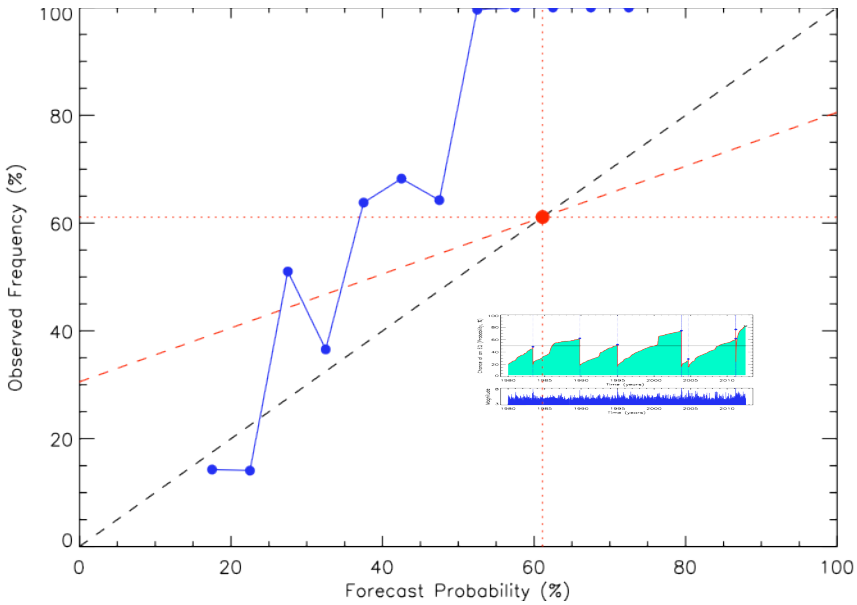

Fig. 9.12: Reliability (scatterplot) diagram for earthquake probabilities corresponding to the timeseries shown in Figure 9.11. In the figure, there are 12 bins having forecast probability, and these are plotted against observed frequencies. A perfectly reliable forecast would have zero reliability error, and the blue dots would lie along the black dashed line having slope = 1. The red dashed line is the no skill line, and the large red dot is the "climatology point", or average forecast. **Inset**: The fraction of samples in each of the 20 forecast bins of 0% to 5%, 5% to 10%, ..., 95% to 100%.

9.6 Results

Applying these ideas to earthquakes in California, we use data from the area between latitudes 29° and 42° north, and between longitudes -127° and -113° degrees west. We consider the time interval from January 1, 1980 until present (July 17, 2012), using data from the ANSS catalog with a catalog completeness level of magnitude $m_s \geq 3.5$. For data analysis and plotting purposes, we use a time step equal to 0.01 year, about 3.65 days. Larger earthquakes closer together in time than this value will not appear independently in the time series plots, although they are treated as separate events in the verification analyses. Examples include the June 28, 1992 Landers-Big Bear events ($m = 7.3$, $m = 6.5$, 3 hours apart), and the November 23-24, 1987 Elmore Ranch-Superstition Hills events ($m = 6.2$, $m = 6.6$, 12.3 hours apart).

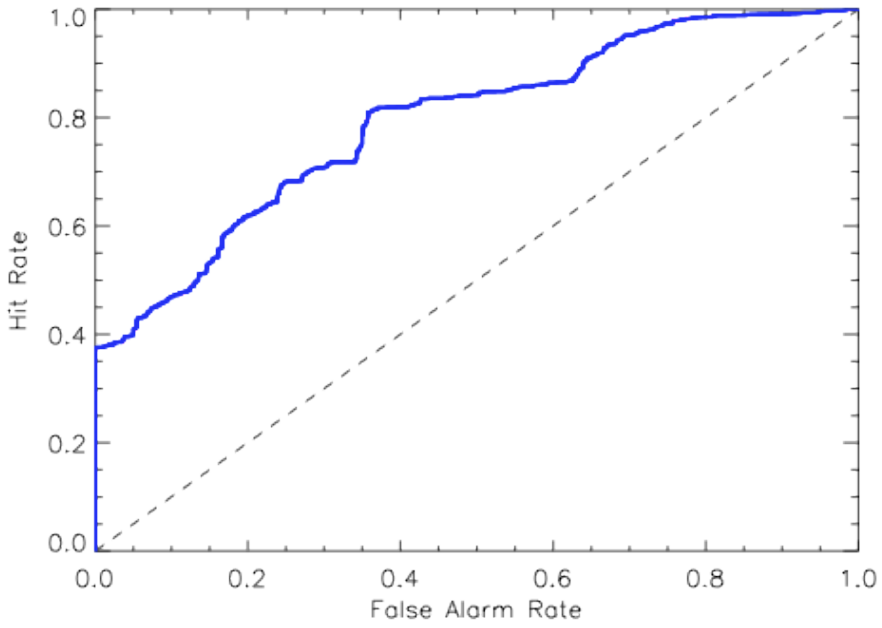

Fig. 9.13: Temporal Receiver Operating Characteristic diagram for the forecast of Figure 9.11. The solid blue line is the ROC diagram for January 1, 1980 through July 17, 2012.

To make practical calculations, we first compute the Poisson rate of small earthquakes $\nu_s(m \geq 3.5)$ in the defined region. Figure 9.6 shows a map of the region, and Figure 9.7 shows the optimal forecast as a function of time in years over the period January 1, 1980 - July 17, 2012. Figure 9.8 is a plot of the Reliability Diagram, and Figure 9.9 is a plot of the Receiver Operating Characteristic. Details are given in Rundle et al. (2012, 2011).

For the backtesting process, we use data only up until 22:40:41.77 GMT on April 4, 2010, the time and date of the $m = 7.2$ El Mayor-Cucapah (Baja) earthquake. The reason is that any forecast arising from any of the data from April 4 until present would automatically be counted as false alarm, since by definition, no earthquake with $m_l \geq 6$ has occurred since April 4, 2010. Therefore, any forecast after April 4, 2010, for example in Figure 9.7, can be considered as an actual future forecast for $m_l \geq 6$ earthquakes within the California-Nevada study area.

In a similar way, we compute a forecast in the Japan region over the period January 1, 1980 - July 17, 2012. This forecast is for $m_l \geq 7.5$ over 4 years (48 months), in the region between latitudes 28° and 42° north, and between longitudes 127° and 146° degrees east. For the Japan calculations, we use $m_s \geq 4.25$, a maximum depth of 40 km (shallow events), and again use a

time step of 0.01 year. The map of large events is shown in Figure 9.10, the forecast is shown in Figure 9.11, and the R/A and ROC curves are shown in Figures 9.12 and 9.13. In the Japan figures, the R/A and ROC curve use data only through 06:25:50.30 GMT on March 11, 2011, the date of the great $m = 9.1$ Tohoku, Japan earthquake. Again, the portion of the forecast in Figure 9.11 would be counted as a false alarm by the R/A and ROC methods if we were to use that data in calculations, so again the forecast since March 11, 2011 represents an actual forecast of future activity.

9.7 Summary

We have discussed the role of scaling and self-organization in both earthquake data and earthquake models. We have also discussed the problem of earthquake forecasting, and show that forecasts can be developed based on the idea of "filling in" a fat-tailed (scaling) distribution. We then show that earthquake forecasts can be computed, with validation and verification based on standard methods in the literature.

As of this writing (July 17, 2012), it can be seen from Figures 9.7 and 9.11 that significant large earthquake activity is expected in the relatively near future in both California-Nevada ($m_l \geq 6$, $\Delta t \leq 1$ year from 2012/7/17) and Japan ($m_l \geq 7.25$, $\Delta t \leq 4$ years from 2012/7/17).

Acknowledgements

Research by MKS was supported by NASA Fellowship NNX11AL92H. Research by JBR and JRH was performed with funding from NASA grant NNX08AF69G to the University of California, Davis.

References

Abaimov, S., Turcotte, D. L., Shcherbakov, R., Rundle, J. B., Yakovlev, G., Goltz, C., & Newman, W. (2008). Earthquakes: Recurrence and interoccurrence times. *Pure and Applied Geophysics*, *165*, 777–795. 10.1007/s00024-008-0331-y.

Alava, M., Nukala, P., & Zapperi, S. (2006). Statistical models of fracture. *Advances in Physics*, *55*(3), 349 – 476.

Ando, M. (1975). Source mechanisms and tectonic significance of historical earthquakes along the nankai trough, japan. *Tectonophys.*, *27*, 119–140.

Bakun, W. H., Aagaard, B., Dost, B., Ellsworth, W. L., Hardebeck, J. L., Harris, R. A., Ji, C., Johnston, M. J. S., Langbein, J., Lienkaemper, J. J., Michael, A. J., Murray, J. R., Nadeau, R. M., Reasenberg, P. A., Reichle, M. S., Roeloffs, E. A.,

Shakal, A., Simpson, R. W., & Waldhauser, F. (2005). Implications for prediction and hazard assessment from the 2004 Parkfield earthquake. *Nature*, *437*, 969–974.

Biasi, G. P., Weldon, R. J., Fumal, T. E., & Seitz, G. G. (2002). Paleoseismic event dating and the conditional probability of large earthquakes on the southern san andreas fault, california. *Bull. Seis. Soc. Am.*, *92*(7), 2761–2781.

Burridge, R., & Knopoff, L. (1967). Model and theoretical seismicity. *Bull. Seis. Soc. Am.*, *57*(3), 341–371.

Carlson, J. M., & Langer, J. S. (1989). Mechanical model of an earthquake fault. *Phys. Rev. A*, *40*(11), 6470–6484.

Dziewoński, A. M., Chou, T. A., & Woodhouse, J. W. (1981). Determination of earthquake source parameters from waveform data for studies of global and regional seismicity. *J. Geophys. Res.*, *86*(B4), 2825–2852.

Ekström, G., Dziewoński, A. M., Maternovskaya, N. N., & Nettles, M. (2005). Global seismicity of 2003: centroid–moment-tensor solutions for 1087 earthquakes. *Phys. Earth Planet. Inter*, *148*, 327–351.

Engdahl, E. R., van der Hilst, R., & Buland, R. (1998). Global teleseismic earthquake relocation with improved travel times and procedures for depth determination. *Bull. Seis. Soc. Am.*, *88*(3), 722–743.

Evans, M., Hastings, N. A. J., & Peacock, J. B. (2000). *Statistical distributions*. Wiley series in probability and statistics. Probability and statistics section. New York: Wiley, 3rd ed. ed.
URL `http://www.loc.gov/catdir/bios/wiley042/99088655.html`

Field, E. H. (2007a). Overview of the working group for the development of regional earthquake likelihood models (RELM). *Seis. Res. Lett.*, *78*, 7–16.

Field, E. H. (2007b). A summary of previous working groups on California earthquake probabilities. *Seis. Soc. Am. Bull.*, *97*, 1033–1053.

Gardner, J. K., & Knopoff, L. (1974). Is the sequence of earthquakes in southern california, with aftershocks removed, poissonian? *Bull. Seis. Soc. Am.*, *64*, 1363–1367.

Green, D. M., & Swets, J. A. (1966). *Signal detection theory and psychophysics*. Huntington, N.Y.: R. E. Krieger Pub. Co.

Guarino, A., Garcimartín, A., & Ciliberto, S. (1998). An experimental test of the critical behaviour of fracture precursors. *The European Physical Journal B - Condensed Matter and Complex Systems*, *6*, 13–24. 10.1007/s100510050521.

Gutenberg, B., & Richter, C. F. (1954). *Seismicity of the Earth and Associated Phenomena*. Princeton, N.J.: Princeton University Press.

Hirose, K. (2012). 2011 fukushima dai-ichi nuclear power plant accident: summary of regional radioactive deposition monitoring results. *J. Env. Radioactivity*, *111*, 13–17.

Hofmann, R. B. (1996). Individual faults can't produce a gutenberg-richter earthquake recurrence. *Engineering Geology*, *43*(1), 5 – 9.

Hsu, W., & Murphy, A. H. (1986). The attributes diagram a geometrical framework for assessing the quality of probability forecasts. *International Journal of Forecasting*, *2*(3), 285 – 293.

Ishibe, T., & Shimazaki, K. (2009). Seismicity in source regions of large interplate earthquakes around japan and the characteristic earthquake model. *Earth Planets and Space*, *61*(9), 1041 – 1052.

Jolliffe, I. T., & Stephenson, D. B. (2011). *Forecast verification: a practitioner's guide in atmospheric science*. Hoboken, NJ: John Wiley and Sons, 2nd ed ed.

Kharin, V. V., & Zwiers, F. W. (2003). On the roc score of probability forecasts. *Journal of Climate*, *16*(24), 4145–4150.
URL `http://dx.doi.org/10.1175/1520-0442(2003)016<4145:OTRSOP>2.0.CO;2`

Kinnison, R. R. (1985). *Applied Extreme Value Statistics*. Columbus, Ohio: Battelle Press.

Lee, Y. T., Turcotte, D. L., Holliday, J. R., Sachs, M. K., Rundle, J. B., Chen, C. C., & Tiampo, K. F. (2011). Results of the regional earthquake likelihood models (RELM) test of earthquake forecasts in California. *Proc. Nat. Acad. Sci. (USA)*, *108*(40), 16533–16538.

Mantegna, R. N., & Stanley, H. E. (2000). *An introduction to econophysics: correlations and complexity in finance*. Cambridge, UK: Cambridge University Press. URL `http://www.loc.gov/catdir/samples/cam034/99028047.html`

Mason, I. B. (1982). A model for assessments of weather forecasts. *Austral. Met. Mag.*, *30*, 291–303.

Murphy, A. H., & Daan, H. (1985). Forecast evaluation. In A. H. Murphy, & R. W. Katz (Eds.) *Probability, Statistics and Decision Making in the Atmospheric Sciences*. Westview Press Boulder, CO.

Murphy, A. H., & Winkler, R. L. (1987). A general framework for forecast verification. *Mon. Weather Rev.*, *115*, 1330–1338.

Rundle, J. B. (1989). Derivation of the complete gutenberg-richter magnitude-frequency relation using the principle of scale invariance. *J. Geophys. Res.*, *94*(B9), 12337–12342.

Rundle, J. B., Holliday, J. R., Graves, W., Turcotte, D. L., Tiampo, K. F., & Klein, W. (2012). Probabilities for large events in driven threshold systems. *Phys. Rev. E*, *86*(021106).

Rundle, J. B., Holliday, J. R., Yoder, M., Sachs, M. K., Donnellan, A., Turcotte, D. L., Tiampo, K. F., Klein, W., & Kellogg, L. H. (2011). Earthquake precursors: activation or quiescence? *Geophysical Journal International*, *187*(1), 225–236.

Sachs, M. K., Yoder, M. R., Turcotte, D. L., Rundle, J. B., & Malamud, B. D. (2012). Black swans, power laws, and dragon-kings: Earthquakes, volcanic eruptions, landslides, wildfires, floods, and soc models. *Eur. Phys. J. Special Topics*, *205*, 167–182.

Scholz, C. H. (1990). Geophysics–earthquakes as chaos. *Nature*, *348*, 197–198.

Scholz, C. H., & Anderson, D. L. (2002). *The Mechanics of Earthquakes & Faulting*. Cambridge: Cambridg University Press, 2nd ed.

Schorlemmer, D., Zechar, J. D., Werner, M. J., Field, E. H., Jackson, D. D., & Jordan, T. H. (2010). First results of the regional earthquake likelihood models experiment. *Pure Ap. Geophys.*, *167*, 859–876.

Shcherbakov, R., Turcotte, D. L., & Rundle, J. B. (2006). Scaling properties of the parkfield aftershock sequence. *Bull. Seis. Soc. Am.*, *96*(4B), S376–384.

Sornette, D. (2004). *Why Stock Markets Crash: Critical Events in Complex Financial Systems*. Princeton University Press.

Sornette, D. (2009). Dragon-kings, black swans and the prediction of crises. *International Journal of Terraspace Science and Engineering*, *2*, 1.

Sornette, D., Knopoff, L., Kagen, Y., & Vanneste, C. (1996). Rank-ordering statistics of extreme events: Application to the distribution of large earthquakes. *J. Geophys. Res.*, *101*(B6), 13883–13893.

Stein, R. S., Barka, A. A., & Dieterich, J. H. (1997). Progressive failure on the north anatolian fault since 1939 by earthquake stress triggering. *Geophysical Journal International*, *128*(3), 594–604. URL `http://dx.doi.org/10.1111/j.1365-246X.1997.tb05321.x`

Taleb, N. (2007). *The Black Swan: The Impact of the Highly Improbable*. New York: Random House, 1st ed ed.

Turcotte, D. L. (1997). *Fractals and Chaos in Geology and Geophysics*. Cambridge, U.K.: Cambridge University Press, 2nd ed ed.

Wesnousky, S. G. (1994). The gutenberg-richter or characteristic earthquake distribution, which is it? *Bull. Seis. Soc. Am.*, *84*(6), 1940–1959.

Yates, R. D., & Goodman, D. J. (2005). *Probability and Stochastic Processes*. New York: John Wiley and Sons.